Single-phase and two-phase cooling characteristics of upward-facing and downward-facing sprays

Jon R. Rybicki, Issam Mudawar *

Boiling and Two-Phase Flow Laboratory, School of Mechanical Engineering, Purdue University, West Lafayette, IN 47907 1288, USA

Abstract

Experiments were performed to ascertain the cooling characteristics of PF-5052 sprays impacting a square heated test surface in an upward orientation. Three full-cone spray nozzles were used to span a broad range of volumetric flux. Also examined were the effects of Sauter mean diameter and subcooling. The present data were compared to prior data for downward-oriented FC-72, FC-87 and water sprays to assess the effects of spray orientation on cooling performance. The combined database facilitated the development of generalized correlations for single-phase heat transfer, nucleate boiling, and critical heat flux (CHF). The nucleate boiling data for different fluids and both upward and downward orientation were fitted using a single correlation based on density ratio, Weber number and Jacob number. A CHF correlation previously developed for downward-oriented sprays was equally successful at predicting the present upward-oriented PF-5052 spray data. Overall, orientation showed no measurable influence on any of the spray cooling regimes examined.
© 2005 Elsevier Ltd. All rights reserved.

1. Introduction

For decades, spray cooling has been used in metal quenching operations in pursuit of controlled microstructural development and superior mechanical properties. Because temperatures in metal processing are quite elevated, much of the early spray cooling literature is associated with the film boiling regime.

However, many emerging technologies, such as computer electronics and defense laser and microwave systems, are demanding the dissipation of large heat fluxes while maintaining relatively low surface temperatures.

This performance is realized by maintaining spray cooling safely within the nucleate boiling regime. While other cooling schemes, such as microchannel flow and jet impingement, can achieve similar results, sprays feature enhanced temperature uniformity across the heat-dissipating surface. By utilizing liquid momentum to break up the liquid into fine droplets, a large increase in the liquid's surface area to volume ratio is achieved. Coupled with a broad dispersion of droplets across the heat-dissipating surface, the increase in liquid surface area makes it possible to achieve high heat transfer coefficients while maintaining the temperature uniformity demanded by modern high-performance devices. Other key merits of droplet dispersion and impact are the ability to resist localized dryout and delay critical heat flux (CHF).

Despite these attributes, there is a general reluctance to incorporate spray cooling in demanding cooling

---
* Corresponding author. Tel.: +1 765 494 5705; fax: +1 765 494 0539.
  E-mail address: mudawar@ecn.purdue.edu (I. Mudawar).

Nomenclature

A	area
Bo	Boiling number
c_p	specific heat
d_o	nozzle orifice diameter
d_{32}	Sauter mean diameter (SMD)
g	acceleration due to gravity
H	nozzle-to-surface distance
h_{fg}	latent heat of vaporization
k	thermal conductivity
L	length and width of square test surface
$Nu_{d_{32}}$	Nusselt number
P	pressure
ΔP	pressure drop across spray nozzle
Pr	Prandtl number
Q	volumetric flow rate
Q''	volumetric spray flux
$\underline{Q''}$	average volumetric spray flux based on circular impact area of spray
q''	surface heat flux based on area of square test surface
q''_{dryout}	maximum heat flux that could possibly be removed by spray
q''_m	average critical heat flux based on area of square test surface
$q''_{m,p}$	local critical heat flux
r	radial distance from centerline of spray
Re_{d_o}	Reynolds number based on nozzle orifice diameter
$Re_{d_{32}}$	Reynolds number based on Sauter mean diameter

T_i	nozzle inlet temperature
T_s	surface temperature
T_{sat}	saturation temperature
ΔT_{sub}	difference between saturation temperature and nozzle inlet temperature, $T_s - T_i$
We_{d_o}	Weber number based on nozzle orifice diameter

Greek symbols

γ	coordinate in spray volumetric flux model
η	evaporation efficiency
θ	spray cone angle
μ	viscosity
ρ	density
σ	surface tension

Subscripts

d_o	based on diameter of nozzle orifice
d_{32}	based on Sauter mean diameter
f	liquid
g	vapor
i	nozzle inlet
m	maximum (CHF)
p	point-based
s	surface
sat	saturation
sub	subcooling

situations. Much of this reluctance is the result of relatively poor understanding of the underlying mechanisms of spray cooling compared to those of competing cooling schemes, such as microchannel flow and jet impingement. A key reason for this poor understanding is the dependence of spray cooling performance on an unusually large number of parameters, such as mean droplet diameter, mean droplet velocity, volumetric flux, and the statistical distributions of these parameters, as well as cone angle and nozzle-to-surface distance. By comparison, the cooling performance of a free jet, for example, is dictated by fewer and more easily measured parameters such as orifice diameter and jet velocity, and is independent of nozzle-to-surface distance [1].

There are other practical concerns with spray cooling, such as the lack of repeatability of cooling performance for seemingly identical nozzles due to any minute manufacturing imperfections or to corrosion or erosion of the nozzle interior [2]. Those concerns can be overcome by using corrosion resistant nozzles and adopting stringent quality control and nozzle characterization practices.

1.1. Spray cooling literature

Spray cooling literature is quite sparse. Toda [3] observed subcooling had only minor effects on single-phase and nucleate boiling heat transfer and did not have a dominant effect on CHF either. Changing the size of the heat-dissipating test surface significantly altered the effects of subcooling on nucleate boiling performance. Increasing subcooling changed the gradient of the nucleate boiling curve for a larger circular surface ($D = 37.7$ mm) but caused a parallel shift in the curve for a small surface ($D = 15.0$ mm). Monde [4] showed the nucleate boiling gradient in spray cooling is nearly half that for pool boiling. Both Toda and Monde showed increasing the spray volumetric flux enhances cooling performance in every cooling regime.

Cho and Wu [5] developed a CHF correlation for Freon-113 sprays based on Weber number but did not account for droplet size. Mudawar and Valentine [6] determined local cooling characteristics for all regimes of the boiling curve (film, transition, and nucleate boiling

as well as single-phase cooling) using water as working fluid. Like Toda and Monde, they showed volumetric flux had the most dominant effect on CHF compared to other hydrodynamic properties of the spray. Holman et al. [7,8] used droplet velocity and droplet diameter as key parameters in correlating nucleate boiling data. Estes and Mudawar [9] developed an empirical relationship for CHF for FC-72, FC-87 and water based on local volumetric flux, Q'', and Sauter mean diameter (SMD), d_{32}, but not droplet speed. Volumetric flux is defined as the flow rate impacting an infinitesimal portion of the surface divided by the area of the same portion. It therefore has the units of velocity. The dimensionless correlation form utilized by Mudawar and Valentine and Estes and Mudawar proves the proper scaling velocity for heat transfer near CHF is Q'', not droplet velocity, and the scaling length is d_{32}. Conversely, Chen et al. [10] concluded d_{32} has a negligible effect on CHF, while droplet velocity is a dominant parameter in CHF determination.

Mudawar and Estes [11] also emphasized the need for consistency in acquiring and comparing spray heat transfer data. Failure to adhere to strict geometrical requirements concerning cone angle and nozzle-to-surface distance was shown to produce drastically different cooling performances which can yield erroneous inferences concerning the effects of individual spray parameters.

In other related studies, Lin and Ponnappan [12] investigated multi-nozzle spray cooling of high power laser diode arrays. They reported CHF values similar to those for single nozzles but using lower flow rates. Rini et al. [13] explained the spray heat transfer mechanism as the combined effect of surface nucleation, secondary nucleation, convection heat transfer to the liquid film, and direct evaporation of the liquid.

The primary purpose of the present study is to develop comprehensive design tools vital to the implementation of spray cooling. These include correlations for single-phase and nucleate boiling regimes as well as CHF for full cone pressure sprays impacting a square heat-dissipating test surface. New data for upward-oriented PF-5052 sprays are compared to prior downward-oriented spray data for FC-72, FC-87 and water in pursuit of generalized correlations that account for the effects of nozzle, fluid, volumetric flux, droplet diameter, and subcooling, in addition to flow orientation. Data were carefully selected which adhere to consistent geometrical requirements recommended earlier by Mudawar and Estes [11].

2. Experimental methods

2.1. Two-phase flow loop

The fluid used in this study, PF-5052, is a dielectric coolant made by 3M company. It features several attributes superior to those of the popular electronic cooling fluid FC-72, such as a lower boiling point of 50 °C at 1 atm (compared to 56 °C for FC-72) and higher values for both surface tension and latent heat of vaporization. Relevant properties of saturated PF-5052 at 1 atm are as follows: $\rho_f = 1643$ kg/m^3, $\rho_g = 12.0$ kg/m^3, $\sigma = 0.013$ N/m, $h_{fg} = 104{,}700$ J/kg, $c_{p,f} = 1092$ J/kg K, $\mu_f = 517 \times 10^{-3}$ N s/m^2, $k_f = 0.058$ W/m K, and $Pr_f = 9.65$.

A closed two-phase flow loop was constructed to deliver PF-5052 at the appropriate pressure, temperature and flow rate as it entered the spray nozzle and impacted a heated test surface situated inside a spray chamber. As shown in Fig. 1, the bulk of the fluid is contained inside a reservoir. Situated beneath the reservoir is a deaeration chamber fitted with an electrical immersion heater that is also used to pre-heat the fluid. The fluid is circulated in the loop with the aid of a magneti-
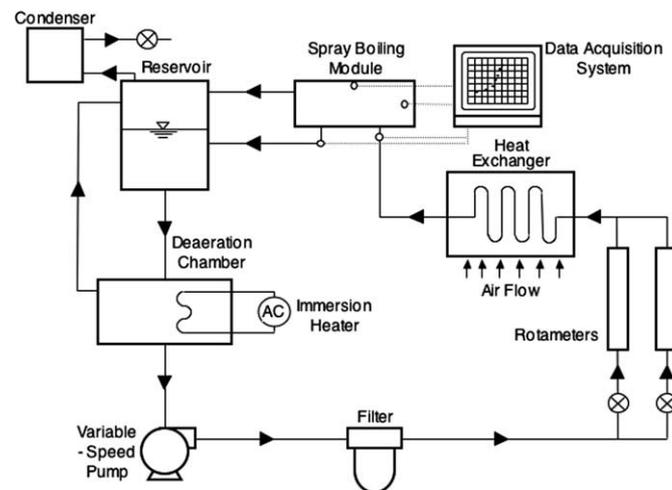
Fig. 1. Two-phase spray cooling flow loop.

cally-coupled centrifugal pump. Downstream from the pump is a filter followed by a pair of rotameters. Fluid exiting the rotameters is passed through a finned-tube heat exchanger that is cooled by two high-capacity fans. The pre-cooled fluid then enters the spray chamber, where it is partially evaporated. The fluid is separated by gravity inside the spray chamber; the liquid and vapor are routed separately into the reservoir. Situated atop the reservoir is a fan-cooled finned-tube condenser to convert the vapor back into liquid state.

2.2. Spray chamber

The spray chamber was designed to permit direct viewing of the spray and test surface. As shown in Fig. 2, the liquid is sprayed vertically upwards upon the test surface. The spray chamber is fabricated mostly from G-10 fiberglass plastic and fitted with transparent front and rear windows made from polycarbonate plastic. The spray nozzle is accurately positioned relative to the impact surface with the aid of a micrometer translation stage. Following the model by Mudawar and Estes [11], the nozzle-to-surface distance is adjusted such that the spray impact area just inscribes the $1.0 \times 1.0 \text{ cm}^2$ area of the test heater. The vapor generated from the spray boiling is routed through two side outlets in the top region of the spray chamber, while the liquid is drained through a third outlet at the bottom. The chamber is fitted with pressure and temperature sensors that are used to measure operating conditions around the spray. Not shown in Fig. 2 are nozzle inlet pressure and temperature sensors that are connected to the tube leading to the spray nozzle. These sensors are used to measure nozzle

inlet conditions; the measured pressure is corrected for hydrostatic height of liquid between the vertical positions of the pressure sensor and nozzle inlet.

This study employed three Unijet full-cone nozzles made by Spraying Systems Company. These nozzles were selected for their relatively wide cone angle and broad range of flow rate necessary for assessment of the effects of key spray hydrodynamic parameters. Each of these pressure spray nozzles contains an internal vane that induces controlled turbulence in the liquid in order to produce the full cone spray pattern without the aid of a secondary air stream. Table 1 shows key hydrodynamic characteristics of the three nozzles.

2.3. Heater construction

As shown in Fig. 3(a) and (b), heat is supplied to the $1.0 \times 1.0 \text{ cm}^2$ test heater area by nine 220 W cartridge heaters that are embedded in an oxygen-free copper block. The copper block is wrapped in a high-temperature insulating blanket; additional insulation is available where the copper block mates with the top G-10 surface of the spray chamber. The thermal capacitance of the

Table 1
Characteristics of spray nozzles utilized in present study

Nozzle	Orifice diameter d_o (mm)	Spray angle θ (°)	Sauter mean diameter $d_{32} \times 10^6$ (m)	Volumetric flux $Q'' \times 10^3$ ($\text{m}^3 \text{ s}^{-1}/\text{m}^2$)
1	0.76	55.8	109–122	35–52
2	1.19	46.4	119–135	83–101
3	1.70	48.5	112–151	113–186
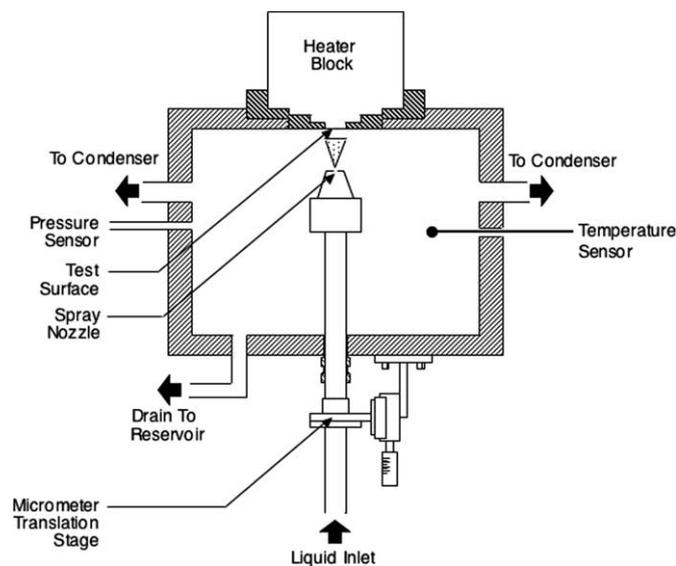
Fig. 2. Schematic of spray chamber.
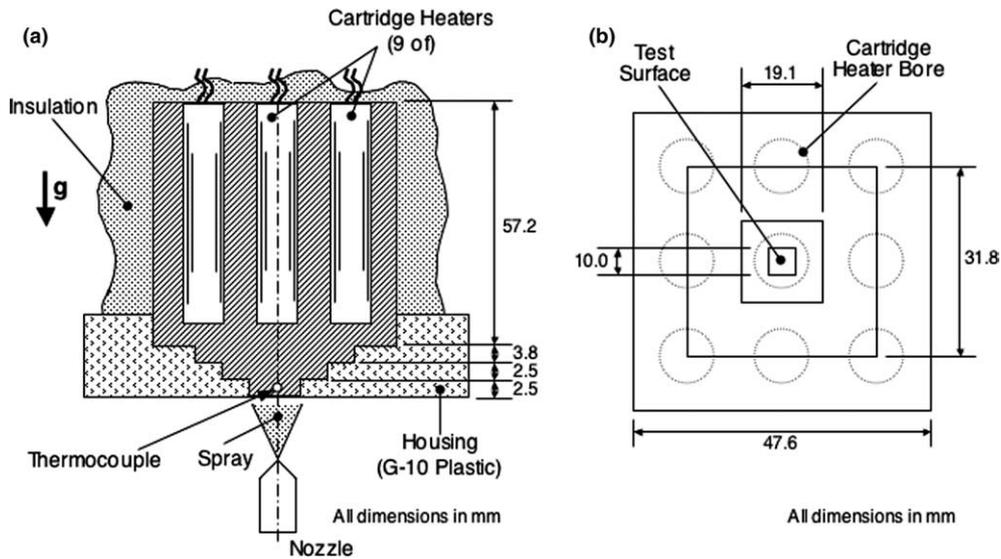
Fig. 3. (a) Longitudinal section of heater assembly and (b) bottom view of copper block.

copper block dampened the temperature excursions associated with CHF detection, providing the operator adequate time to cut-off electrical power input to the cartridge heaters with no risk of physical burnout of the heater materials.

Electrical power was supplied to the cartridge heaters by a variable voltage transformer and measured with a 0.5% accuracy Yokogawa digital wattmeter. Thermal analysis showed the heater insulation insured less than 2% of the electrical power input was lost to the ambient during the single-phase liquid cooling regime. The percentage heat loss decreased with increasing power input. The heat supplied to the spray through the 1.0×1.0 cm^2 test surface was therefore assumed equal to the electrical power input. Fig. 3(a) shows a type-K (Chromel–Alumel) thermocouple embedded 1.27 mm above the test surface. The signal from this thermocouple, as well as from temperature and pressure sensors throughout the loop, were recorded and processed by an HP 3497A digital acquisition/control system. A three-dimensional heat diffusion model using FLUENT showed the surface temperature was very close to that inferred using one-dimensional heat conduction between the planes of the thermocouple and the test surface. The assumption of one-dimensional conduction was therefore used to determine test surface temperature throughout the study. The largest difference between surface temperatures using the two methods was 3.2 °C, corresponding to the low heat flux range of the single-phase cooling regime.

2.4. Operating procedure

A consistent test procedure was adopted to ensure consistency between tests corresponding to different noz-zles and operating conditions. The fluid was carefully deaerated to ensure any dissolved non-condensable gases were expelled to the ambient before any experiments were carried out. This was accomplished by first bringing the liquid in the deaeration chamber to a vigorous boil for about 30 min. The vapor generated, mixed with the non-condensable gases, traveled upwards through the reservoir and into the condenser, where the PF-5052 vapor was recovered by condensation while the superfluous gases escaped freely to the ambient. The pump was then turned on and the deaeration process continued for an additional 30 min while the fluid was circulated through the loop. Afterwards, the condenser's vent valve was closed off, sealing the loop fluid from the ambient. Experiments involving high subcooling required an additional 10–15 min of pre-cooling using the finned-tube heat exchanger. The spray chamber was maintained at atmospheric pressure throughout the study.

Boiling curves were generated by raising the voltage across the cartridge heaters in small increments and recording the heat flux from the test surface, the surface temperature, and the nozzle inlet temperature. The boiling data were recorded only after the heater temperature reached steady state, which was confirmed by a less than 0.1 °C temperature change over a 10 min period. Smaller voltage increments were applied near CHF to both preclude premature CHF occurrence and enhance CHF measurement accuracy. CHF was detected by a rapid unsteady rise in the surface temperature resulting from a small voltage increment. Thereafter, the power supply was manually cut-off and the heater allowed to cool down.

Uncertainties in the pressure, flow rate and temperature measurements were less than 0.5%, 1.0% and ±0.2 °C, respectively.

3. Configuration and hydrodynamic characterization of spray

As indicated earlier, the cooling performance of a spray is dependent on two key hydrodynamic parameters: volumetric flux, Q'', and Sauter mean diameter, d_{32}. Below is a discussion of how these parameters were determined.

Mudawar and Estes [11] provided a detailed study of the spatial variations of the spray's volumetric flux for a full-cone spray nozzle. They modeled the nozzle orifice as a uniform point source for fluid flow, i.e. equal volumetric flux is encountered along any spherical surface within the cone angle of the spray that is centered at the point source. Fig. 4 illustrates how a constant volumetric flux along a spherical surface of radius equal to the nozzle-to-surface distance would yield a non-uniform volumetric flux distribution along the heated surface. The model yields an expression for the ratio of local volumetric flux, Q'', at any point along the heated surface to the volumetric flux averaged over the impact area, $\overline{Q}''$, as a function of nozzle-to-surface distance, H, radial location, r, from the center of, and along the heated surface, and spray cone angle, θ.

$$\frac{Q''}{\overline{Q}''} = \frac{1}{2}\left[\frac{\tan^2(\theta/2)}{1-\cos(\theta/2)}\right]\frac{1}{\left[1+\left(\frac{r}{H}\right)^2\right]^{3/2}}, \qquad (1)$$

where the mean volumetric flux is the total spray flow rate divided by the impact area,

$$\overline{Q}'' = \frac{Q}{\pi\{H\tan(\theta/2)\}^2}. \qquad (2)$$

This model predicts a higher flow rate at the center of the spray impact area compared to the circumference of the same area. These spatial variations have a strong bearing on both cooling uniformity and CHF. The relatively low flux in the outer regions means CHF would commence locally at the circumference. This behavior is also dependent on the radius, $H\tan(\theta/2)$, of the spray impact area relative to the length, L, of the heated surface. Mudawar and Estes [11] demonstrated experimentally how a large nozzle-to-surface distance causes a significant portion of the spray droplets to fall outside of the heated area. Conversely, a small distance yields a small droplet impact area, depriving much of the heated test surface from the advantages of direct droplet impact. Both extremes yielded relatively poor CHF values, and CHF was highest when the impact area just inscribed the square heated surface, i.e. when

$$H\tan(\theta/2) = L/2 \qquad (3)$$

and

$$\overline{Q}'' = \frac{Q}{\left(\pi\dfrac{L^2}{4}\right)}. \qquad (4)$$

Eq. (3) provides a very important criterion for configuring a spray cooling system since (i) it is simple to use, (ii)
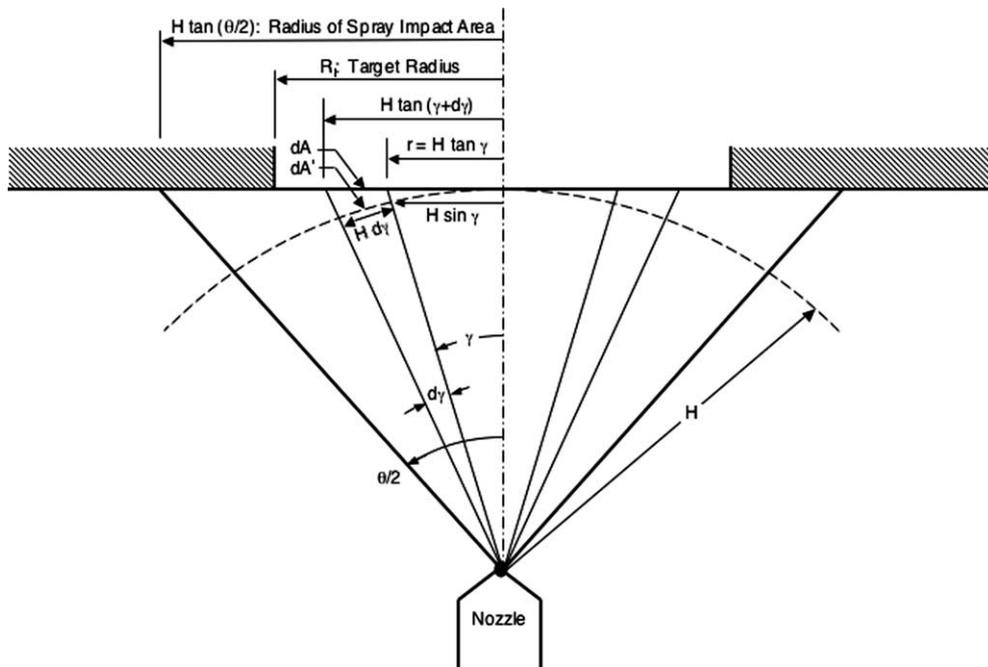
Fig. 4. Spray volumetric flux distribution for uniform point source (adapted from Mudawar and Estes [11]).

it is highly effective at maximizing cooling performance, and (iii) it ensures consistency in acquiring spray heat transfer data. This criterion was therefore adopted throughout the present study.

Estes and Mudawar [9] also developed the following correlation for Sauter mean diameter for full-cone spray nozzles, which was validated for FC-72, FC-87 and water.

$$\frac{d_{32}}{d_o} = 3.67[We_{d_o}^{1/2} Re_{d_o}]^{-0.259}, \tag{5}$$

where We_{d_o} and Re_{d_o} are defined, respectively, as

$$We_{d_o} = \frac{\rho_g (2\Delta P/\rho_f) d_o}{\sigma} \tag{6}$$

and

$$Re_{d_o} = \frac{\rho_f (2\Delta P/\rho_f)^{1/2} d_o}{\mu_f} \tag{7}$$

and ΔP and d_o are the nozzle pressure drop and nozzle orifice diameter, respectively. Eqs. (5)–(7) were used in the present study to determine Sauter mean diameter for the PF-5052 sprays.

4. Experimental results

4.1. Boiling curves

Boiling curves were measured for each of the three nozzles at different flow rates and different subcoolings to explore the effects of these parameters and the spray hydrodynamic parameters on both the single-phase and two-phase regions as well as CHF. Fig. 5(a)–(c) show the effects of flow rate for the three nozzles corresponding to 27 °C inlet subcooling. The relatively small flow range for each nozzle is the result of both nozzle and flow loop limitations. The indicated range for each nozzle ensured fully-developed spray behavior, evidenced by both the spray cone angle and droplet breakup pattern. Fig. 5(a)–(c) show increasing flow rate generally enhances single-phase heat transfer and CHF, but the effect on the nucleate boiling region is relatively modest. Fig. 6(a)–(c) shows the effects of subcooling for a fixed flow rate for the three nozzles. This effect is weak in the single-phase region, brought about mostly by the relatively minor temperature effects on surface tension and liquid viscosity. A noticeable shift in the nucleate boiling region is the result of using the liquid inlet temperature instead of the saturation temperature in plotting the boiling data. Like flow rate, increasing subcooling yields a monotonic increase in CHF for each of the three nozzles.
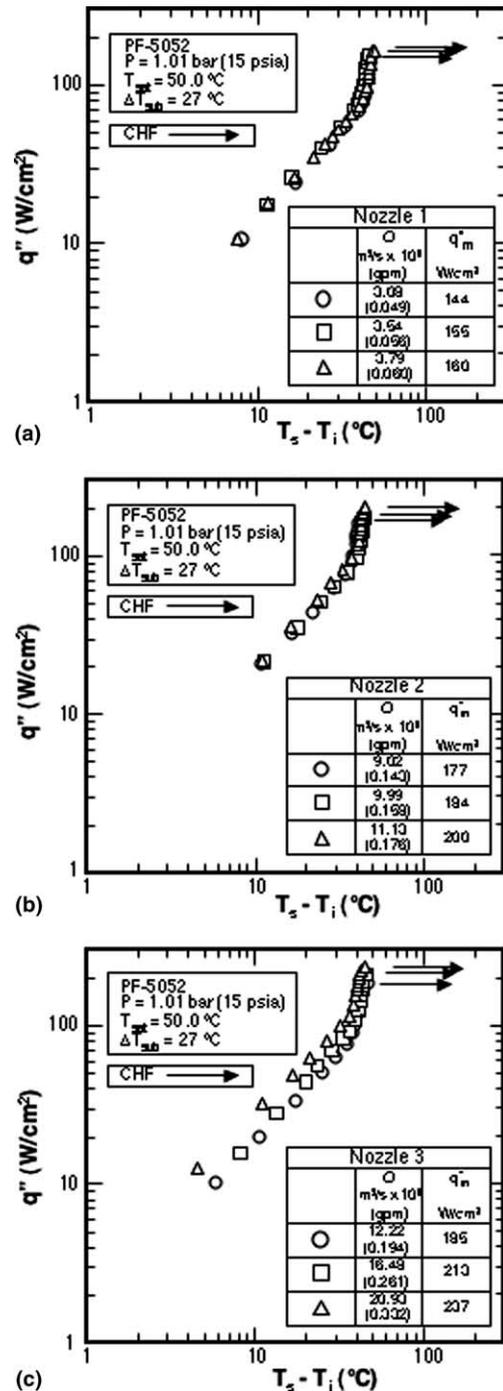
Fig. 5. Boiling curves for different flow rates at $\Delta T_{sub} = 27$ °C for (a) nozzle 1, (b) nozzle 2, and (c) nozzle 3.

In the following sections, the present data are combined with prior data for different fluids to generate correlations for the different regions of the boiling curve. Recall that the present PF-5052 data are for upward-oriented
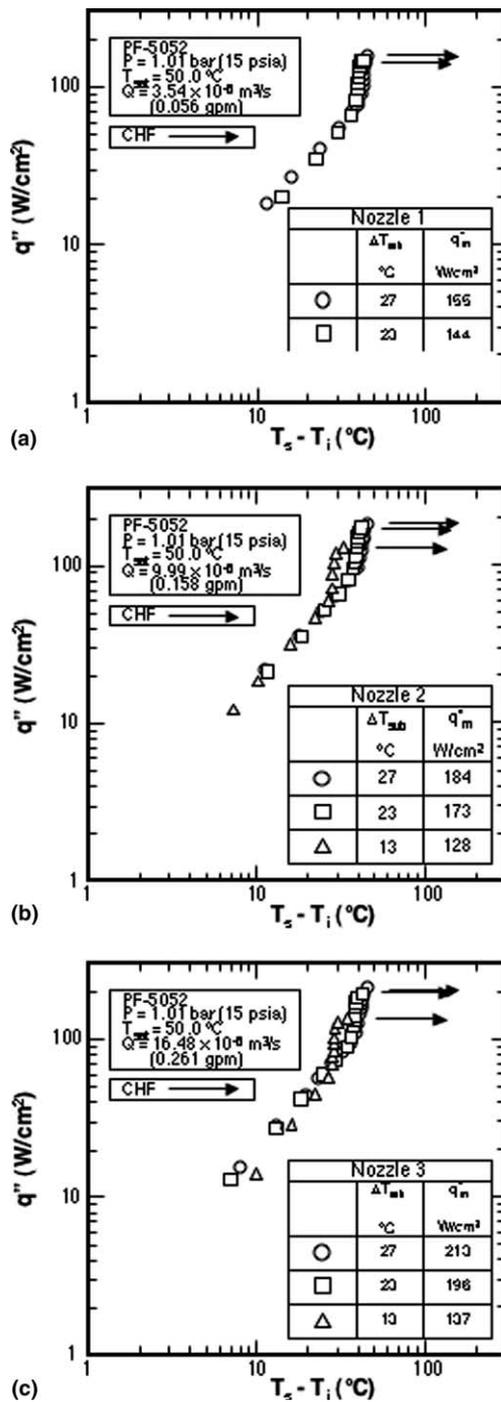
Fig. 6. Boiling curves for different subcoolings for (a) nozzle 1, (b) nozzle 2, and (c) nozzle 3.

sprays while the previous data (FC-72, FC-87 and water) are for downward-oriented sprays. As indicated later in this paper, flow orientation does not appear to influence spray cooling performance, provided the downward-fac-

ing sprays are configured to preclude liquid build-up upon the heated surface.

4.2. Single-phase heat transfer

Single-phase spray data were obtained in the present PF-5052 study for subcoolings ranging from 12 to 27 °C and flow rates from 3.08×10^{-6} to 20.93×10^{-6} m³/s. Increasing flow rate (also volumetric flux) yielded better cooling performance. A similar trend was observed when decreasing the droplet diameter, although it was difficult to achieve common flow rates for different nozzles.

To develop data over a relatively broad range of spray parameters, the present single-phase PF-5052 data were combined with the downward-oriented water spray data of Mudawar and Valentine [6]. Aside form the different spray orientation, the water data were measured using a circular test heater centered in a much larger spray impact area. The volumetric flux for the water data was measured locally using a sampling device with an inlet area equal to that of the heated test surface. For the present PF-5052 data, Eq. (4) was used to determine a mean volumetric flux. Fig. 7 shows the single-phase data for both fluids fitted to the correlation

$$Nu_{d_{32}} = 4.70 Re_{d_{32}}^{0.61} Pr_{\mathrm{f}}^{0.32} \tag{8}$$

with an overall mean absolute error of 13.1%. The Nusselt and Reynolds numbers in Eq. (8) are defines as

$$Nu_{d_{32}} = \frac{q''}{T_{\mathrm{s}} - T_{\mathrm{i}}} \frac{d_{32}}{k_{\mathrm{f}}} \tag{9}$$

and

$$Re = \frac{\rho_{\mathrm{f}} \overline{Q}'' d_{32}}{\mu_{\mathrm{f}}} \tag{10}$$

and all liquid properties are evaluated at the average of the heater surface and liquid inlet temperatures.

4.3. Nucleate boiling heat transfer

Because it is difficult to observe near-wall effects within the spray impact area, nucleate boiling data were extracted from boiling curves by excluding the region close to the point of transition between the single-phase and nucleate boiling regimes. Also excluded from the nucleate boiling database was the region of heat transfer degradation just preceding CHF.

Nucleate boiling data for the present upward-oriented PF-5052 sprays were combined with the downward-oriented water spray data of Mudawar and Valentine to cover a broad range of fluid properties
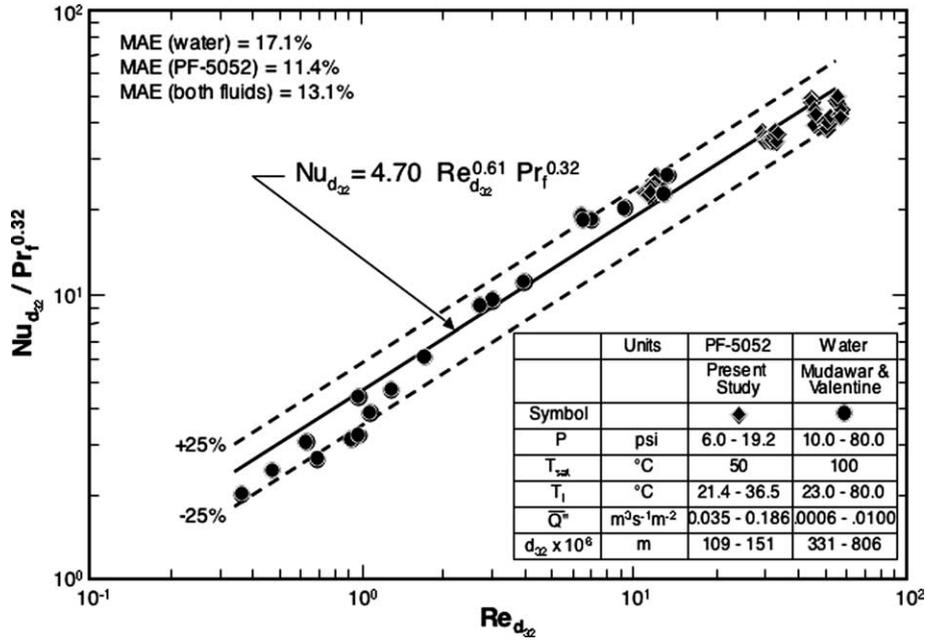
Fig. 7. Single-phase heat transfer correlation for upward-oriented PF-5052 sprays and downward-oriented water sprays.
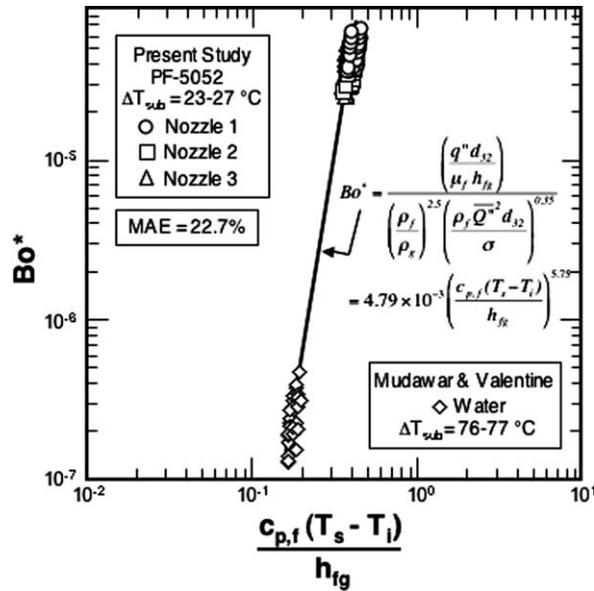
Fig. 8. Nucleate boiling correlation for upward-oriented PF-5052 sprays and downward-oriented water sprays.

and subcoolings. Fig. 8 shows the data for both fluids fitted with a mean absolute error of 22.7% to the correlation

$$Bo^* = 4.79 \times 10^{-3} \left(\frac{c_{p,f}(T_s - T_i)}{h_{fg}} \right)^{5.75}, \tag{11}$$

where

$$Bo^* = \frac{\left(\frac{q'' d_{32}}{\mu_f h_{fg}} \right)}{\left(\frac{\rho_f}{\rho_g} \right)^{2.5} \left(\frac{\rho_f \overline{Q}''^2 d_{32}}{\sigma} \right)^{0.35}}. \tag{12}$$

This correlation form is somewhat similar to one suggested earlier by Holman and Kendall [8] but modified here with a density ratio multiplier and the use of Sauter mean diameter as characteristic length.

4.4. CHF and evaporation efficiency

Estes and Mudawar [9] used a correlation form developed earlier for water sprays by Mudawar and Valentine [6] to fit data for three different fluids. Since the volumetric flux is smallest at the circumference of the spray impact area, Estes and Mudawar based this correlation on the value of volumetric flux at the circumference to determine a point-based CHF, $q''_{m,p}$, at the same location. They successfully fitted their FC-72 and FC-87 data with Mudawar and Valentine's water data according to the correlation

$$\frac{q''_{m,p}}{\rho_g h_{fg} \overline{Q''}} = 2.3 \left(\frac{\rho_f}{\rho_g}\right)^{0.3} \left(\frac{\rho_f Q''^2 d_{32}}{\sigma}\right)^{-0.35} \left(1 + 0.0019 \frac{\rho_f c_{p,f} \Delta T_{sub}}{\rho_g h_{fg}}\right). \tag{13}$$

Eq. (13) can be used to determine the measured CHF data (based on the area of the square test surface) in terms of the mean volumetric flux according to the following transformation [11]:

$$q''_{m,p} = q''_m \frac{L^2}{\left(\frac{\pi}{4} L^2\right)} = \frac{4}{\pi} q''_m \tag{14}$$

and

$$\frac{Q''}{\overline{Q''}} = \frac{1}{2}\{1 + \cos(\theta/2)\} \cos(\theta/2). \tag{15}$$

Eq. (15) was derived by substituting $r = H\tan(\theta/2)$ in Eq. (1).

The present PF-5052 data are plotted in Fig. 9 along with the prior FC-72, FC-87 and water data and the Estes and Mudawar correlation. Recall that all the prior data are for downward-oriented sprays while the PF-5052 data are for upward-oriented sprays. Fig. 9 shows all the present and previous data well predicted by the original Estes and Mudawar correlation, evidenced by a mean absolute data of 14.1%. This proves spray orientation has virtually no effect on CHF.

Evaporation efficiency is another important measure of spray cooling performance. It is defined as the percentage of the maximum heat that could possibly be removed by the spray that was actually removed at CHF.

$$\eta = \frac{q''_m}{q''_{dryout}} \times 100\%$$

$$= \frac{q''_m}{\rho_f \overline{Q''} h_{fg}(1 + c_{p,f}\Delta T_{sub}/h_{fg})} \times 100\%. \tag{16}$$

	Present Study			Estes & Mudawar (1996)			Mudawar & Valentine (1989)
	PF-5052, P = 1.01 bar, T_{sat} = 50°C			FC-72, P = 1.03 bar, T_{sat} = 57.3°C FC-87, P = 1.03 bar, T_{sat} = 30.7°C			Water, P = 1.01 bar, T_{sat} = 100°C
	Nozzle 1	Nozzle 2	Nozzle 3	Nozzle 1	Nozzle 2	Nozzle 3	Several full cone spray nozzles
	●	■	▲	○/⊕	□	△	◇
Q"	35 – 42	83 – 101	113 – 185	16.6 – 52.4 16.6 – 49.7	55.6 – 145	86.3 – 216	0.600 - .0.216
d_{32}	102 - 111	146 - 165	166 - 129	140 - 196 110 - 195	181 - 225	182 - 214	405 - 1350
ΔT_{sub}	22 - 28	12 - 28	12 - 28	13 - 33 4 - 15	13 - 33	13 - 33	20 - 77

Fig. 9. Correlation of CHF data for all fluids, orientations and nozzles based on volumetric flux at outer circumference of impact area.
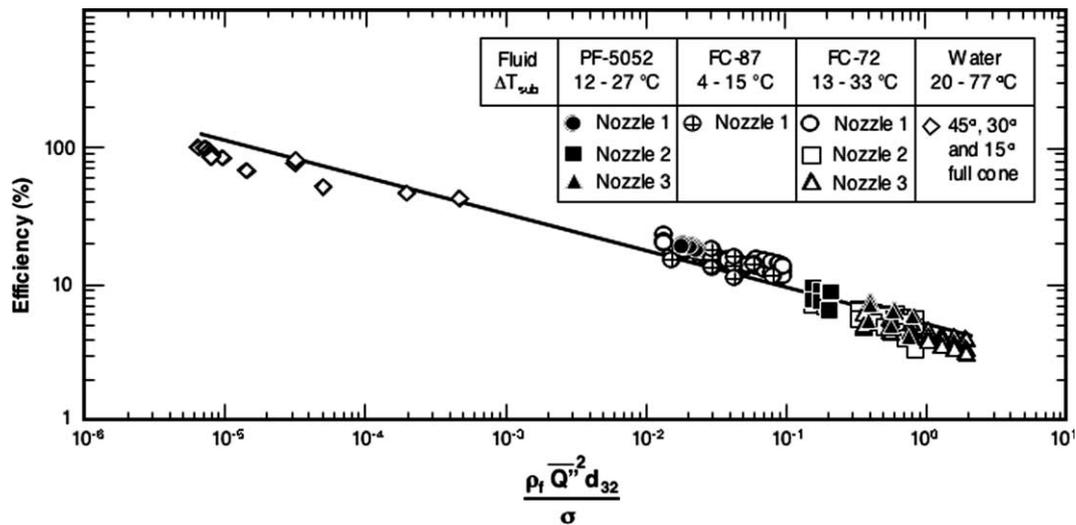
Fig. 10. Evaporation efficiency versus Weber number. PF-5052 data are for upward-oriented sprays, FC-87, FC-72 and water downward-oriented.

The present PF-5052 efficiency data are plotted in Fig. 10 along with previous efficiency data for FC-72, FC-87 and water versus Weber number. This figure shows evaporation efficiency decreases with increasing Weber number, i.e. with increases in volumetric flux and droplet diameter. Agreement between the present upward-oriented PF-5052 spray data and those of downward-oriented sprays of the other three fluids is further proof of the negligible effect of orientation on spray cooling performance.

5. Conclusions

This study investigated the cooling characteristics of pressure sprays impacting a square heated test surface. New data were generated for PF-5052 using three upward-oriented full-cone spray nozzles subject to variations in both flow rate and subcooling. The present data were compared to prior data for downward-oriented sprays using FC-72, FC-87 and water to assess the effects of spray orientation on cooling performance. The combined database was used to develop generalized correlations for single-phase heat transfer, nucleate boiling, and CHF. Key findings from this study are as follows:

(1) Single-phase heat transfer data for different fluids and both upward-oriented and downward-oriented sprays can be fitted using a single correlation based on spray Reynolds number and liquid Prandtl number. Both the Nusselt and Reynolds numbers in this correlation employ Sauter mean diameter as length scale and the average volumetric flux is used as velocity scale in the Reynolds number.

(2) Nucleate boiling data for different fluids and both upward-oriented and downward-oriented sprays can be fitted using a single correlation based on density ratio, Weber number and Jacob number.

(3) A CHF correlation previously developed by Estes and Mudawar [9] for downward-oriented sprays is equally successful at predicting the present upward-oriented PF-5052 spray data. This correlation is based on the assumption that CHF commences at the region of smallest volumetric flux, i.e. the circumference of the impact area.

(4) Volumetric flux and Sauter mean diameter are the key hydrodynamic parameters that influence spray cooling performance.

(5) The present study proves orientation has virtually no effect on spray cooling performance, provided the cooling system does not promote liquid build-up upon the test surface.

References

[1] K.A. Estes, I. Mudawar, Comparison of two-phase electronic cooling using free jets and sprays, J. Electron. Packaging 117 (1995) 323–332.

[2] D.D. Hall, I. Mudawar, Experimental and numerical study of quenching complex-shaped metallic alloys with multiple, overlapping sprays, Int. J. Heat Mass Transfer 38 (1995) 1201–1216.

[3] S. Toda, A study in mist cooling (1st report: investigation of mist cooling), Trans. JSME 38 (1972) 581–588.

[4] M. Monde, Critical heat flux in saturated forced convection boiling with an impinging droplet, Trans. JSME 46 (1980) 1146–1155.

[5] C.S.K. Cho, K. Wu, Comparison of burnout characteristics in jet impingement cooling and spray cooling, in: Proc.

National Heat Transfer Conference, Houston, TX, 1988, pp. 561–567.

[6] I. Mudawar, W.S. Valentine, Determination of the local quench curve for spray-cooled metallic surfaces, J. Heat Treating 7 (1989) 107–121.

[7] M. Ghodbane, J.P. Holman, Experimental study of spray cooling with Freon-113, Int. J. Heat Mass Transfer 34 (1991) 1163–1174.

[8] J.P. Holman, C.M. Kendall, Extended studies of spray cooling with Freon-113, Int. J. Heat Mass Transfer 36 (1993) 2239–2241.

[9] K.A. Estes, I. Mudawar, Correlation of Sauter mean diameter and critical heat flux for spray cooling of small surfaces, Int. J. Heat Mass Transfer 38 (1995) 2985–2996.

[10] R.-H. Chen, L.C. Chow, J.E. Navedo, Effects of spray characteristics on critical heat flux in subcooled water spray cooling, Int. J. Heat Mass Transfer 45 (2002) 4033–4043.

[11] I. Mudawar, K.A. Estes, Optimizing and predicting CHF in spray cooling of a square surface, J. Heat Mass Transfer 118 (1996) 672–680.

[12] L. Lin, R. Ponnappan, Heat transfer characteristics of spray cooling in a closed loop, Int. J. Heat Mass Transfer 46 (2003) 3737–3746.

[13] D.P. Rini, R.-H. Chen, L.C. Chow, Bubble behavior and nucleate boiling heat transfer in saturated FC-72 spray cooling, J. Heat Transfer 124 (2002) 63–72.